# An optimized MNK1b aptamer, apMNKQ2, and its potential use as a therapeutic agent in breast cancer

C. Pinto-Díez,[1,4,5] R. Ferreras-Martín,[1,5] R. Carrión-Marchante,[1] J.I. Klett-Mingo,[1] M. García-Hernández,[1] M.I. Pérez-Morgado,[1] S. Sacristán,[1] M. Barragán,[1] M. Seijo-Vila,[2] I. Tundidor,[2] S. Blasco-Benito,[2] E. Pérez-Gómez,[2] I. Gómez-Pinto,[3] C. Sánchez,[2] C. González,[3] V.M. González,[1] and M.E. Martín[1]

[1]Grupo de Aptámeros, Departamento de Bioquímica-Investigación, IRYCIS-Hospital Universitario Ramón y Cajal, Carretera de Colmenar Viejo Km. 9.100, 28034 Madrid, Spain; [2]Department Biochemistry and Molecular Biology, School of Biology, Complutense University and Instituto de Investigación Hospital 12 de Octubre, 28040 Madrid, Spain; [3]Instituto de Química Física 'Rocasolano', CSIC, 28006 Madrid, Spain

**Breast cancer is the most commonly diagnosed and leading cause of cancer death among women worldwide. Mitogen-activated protein kinase-interacting kinases (MNKs) promote the expression of several oncogenic proteins and are overexpressed in several types of cancer. In human cells, there are four isoforms of MNKs. The truncated isoform MNK1b, first described in our laboratory, has a higher basal activity and is constitutively active. Aptamers are emerging in recent years as potential therapeutic agents that show significant advantages over drugs of other nature. We have previously obtained and characterized a highly specific aptamer against MNK1b, named apMNK2F, with a dissociation constant in the nanomolar range, which produces significant inhibition of proliferation, migration, and colony formation in breast cancer cells. Furthermore, its sequence analysis predicted two G-quadruplex structures. In this work, we show the optimization process of the aptamer to reduce its size, improving its stability. The obtained aptamer, named apMNKQ2, is able to inhibit proliferation, colony formation, migration, and invasion in breast cancer cells. In murine models of breast cancer, apMNKQ2 has demonstrated its efficacy in reducing tumor volume and the number of metastases. In conclusion, apMNKQ2 could be used as an anti-tumor drug in the future.**

## INTRODUCTION

Breast cancer is a heterogeneous disease that affects women at any age after puberty. In 2020, there were 2.3 million women diagnosed with breast cancer, and it has become the most commonly diagnosed cancer and the leading cause of cancer death among women worldwide.[1]

The mitogen-activated protein kinase (MAPK)-interacting kinases (MNKs) have been shown to bind to and to be a substrate for both the mitogen activated extracellular signal-regulated protein kinases (ERK) 1/2 and the stress-activated p38 MAP MAPKs both

in vitro and in vivo.[2] In human cells, there are four MNKs isoforms (MNK1a/b and MNK2a/b), derived from two genes by alternative splicing. The isoform MNK1b, first described by our laboratory, is a truncated isoform lacking the MAPK-binding motif present in the C-terminal region of MNK1a that arises from an alternatively spliced transcript of the *MKNK1* gene.[3] MNK1b has a higher basal activity than MNK1a and its activity does not correlate with the phosphorylation of the activation loop residues, being independent of the upstream kinases (ERK1/2 and p38 MAPK).[3,4] The only well characterized substrate for MNK1 is the eukaryotic initiation factor 4E (eIF4E), but other substrates have been described: nuclear heterogeneous ribonucleoprotein 1,[5] the splicing factor associated with polypyrimidine stretch-binding protein,[6] phospholipase A2,[7] and Sprouty.[8]

Much evidence supports the role of MNKs in oncogenic transformation, metastasis, and tumor progression.[9] MNKs, via eIF4E phosphorylation, promote the expression of several oncogenic proteins, such as vascular endothelial growth factor and fibroblast growth factor, which induce angiogenesis; BCL2, MCL1, and XIAP, with an important role in cell mortality; metalloproteases (MMP) involved in invasion; and cMyc, cyclin D1, ornithine decarboxylase, and HDM2, which regulate cell growth.[10–13] Both MNKs and phosphorylated eIF4E are overexpressed in different types of cancer such as glioblastoma, lymphoma,

breast, prostate, and ovarian cancers, as well as hepatocellular carcinoma, and its high levels of expression are associated with a worse prognosis.[10,14–20] Furthermore, the fact that MNKs are not essential[21] seems to be a good opportunity for pharmacological inhibitors directed against MNK to provide an effective anti-tumor strategy that is not harmful to non-tumor cells. Different MNK inhibitors have been developed in the last years[9,22–24] and two of them (BAY 1143269 from Bayer and eFT508 from eFFECTOR) are currently in clinical phase testing. However, many of these inhibitors are not very specific, producing multiple unwanted side effects and making the establishment of their mechanism of action difficult.

Aptamers are structured polynucleotide sequences (single-stranded DNA [ssDNA] and RNA) isolated from randomized oligonucleotide libraries by the systematic evolution of ligands by exponential enrichment technology, which selectively binds to target molecules with high affinity and specificity[25,26] and that have dissociation constants in the nanomolar range. Furthermore, aptamers have several advantages over antibodies because of the nature of nucleic acids, such as increased stability, easy regeneration, and simple modifications with different reporters during their synthesis. In addition, they are significantly smaller, can be isolated rapidly *in vitro*, and do not trigger a meaningful immune response.[27,28] Aptamers have high potential as therapeutic agents.[24,29,30] However, although there are many other aptamers in different phases of clinical studies, only two have entered into clinical trials for cancer therapy: AS1411 and NOX-A12.

In our laboratory, we selected and characterized aptamers against MNK1b. Among them, the apMNK2F aptamer was able to inhibit proliferation, migration, and colony formation in MDA-MB-231 breast cancer cells.[31] In this work, to enhance the therapeutic capacity of the aptamer and improve its stability and the possibility of reaching its target more easily, we have optimized the apMNK2F aptamer by eliminating dispensable regions of its sequence. In this way, we have obtained an aptamer, named apMNKQ2, that is smaller (only 29 nt), has greater stability and specificity, and maintains the activity of the parental aptamer. Thus, apMNKQ2 is able to inhibit molecular processes characteristic of tumor cells, both in terms of tumorigenic (proliferation, inhibition of apoptosis, and colony formation) and metastatic activity (migration and invasion) in breast tumor cells. Finally, in murine models of breast cancer, apMNKQ2 has demonstrated significant efficacy decreasing tumor growth and the number of metastases. In conclusion, apMNKQ2 could be used as an anti-tumor drug in the future.

## RESULTS

### apMNKQ2, a new optimized version of aptamer apMNK2F

The apMNK2F aptamer previously described in our laboratory[31] has been modified to decrease its size and increase its stability and/or its resistance to nucleases. The sequence predicted by mFold for apMNK2F suggested that the first 18 nucleotides at the 5′ end and the last 14 nucleotides at the 3' end were not involved in the secondary structure of the aptamer or in the G-quadruplex structures predicted with the QGRS Mapper program.[31] Based on this, we designed a

modified apMNK2F, named apMNK2FT, deleting those nucleotides not involved in the structure and adding five thymines in the 5′ end to separate the labeling molecule from the G-quadruplex structure and avoid any potential interference (Figure 1A). G-quadruplex formation in the new aptamer, which contains 48 nucleotides, was experimentally confirmed by $^1$H nuclear magnetic resonance (NMR) and circular dichroism (CD) spectroscopy (Figure 1B). The signals in the 11–12 parts per million region correspond with guanine imino protons involved in G-tetrads and are a clear indication of G-quadruplex formation. Moreover, the positive band around 260 nm and the negative one at 240 nm in the CD spectra are characteristic of a parallel G-quadruplex topology. These results are in agreement with the structural characteristics predicted by mFold (Figure 1A), which suggests a theoretical free energy slightly lower than the original aptamer (−2.64 vs. −3.08 for apMNK2F). Maintenance of the G-quadruplex structure is probably the cause for the new aptamer to keep its ability to bind MNK1 isoforms with high affinity (Figure 1C). However, apMNK2FT is much less effective than apMNK2F inhibiting tumor cell characteristics, such as proliferation or migration, but not colony formation, in the breast cancer cell line MDA-MB-231 (Figures S1A–S1D).

A detailed analysis using QGRS Mapper software predicted four different sequences from apMNK2FT, based on their capacity to form G-quadruplex structures (Figure 2A). These sequences, named apMNKQ1, apMNKQ2, apMNKQ3, and apMNKQ4, have 18, 29, 13, and 22 nucleotides, respectively. Although with different stability, the four sequences exhibit a tendency to form G-quadruplexes as shown by NMR spectroscopy (Figure S2). The effect of the four sequences on the proliferation of three breast cancer cell lines, including two triple-negative cell lines (MDA-MB-231 and MDA-MB-468) and the Luminal A cell line MCF7, was analyzed by 3-[4,5-dimethylthiazol-2-yl]-2,5-diphenyl tetrazolium bromide (MTT) activity assay (Figure 2B). For this, cells were transfected with the different aptamers at 250 nM and MTT activity was measured after 48 h. The results showed that the only aptamer able to inhibit MTT activity at this concentration in the three breast cancer cell lines studied was apMNKQ2. In addition, apMNKQ2 was also the most efficient to inhibit proliferation in other types of cancer cell lines, such as lung cancer (results not shown). For this reason, we have selected the apMNKQ2 aptamer for further characterization and anti-tumoral activity study.

First, we analyzed the stability and resistance to degradation by nucleases. For this, apMNKQ2FT and apMNKQ2 were incubated with several dilutions of DNAse I endonuclease (Figure S3A) for 5 min. No degradation was observed at the different concentrations tested (stability 100%), in contrast with apMNK2FT, which was degraded by more than 90% (Figure S3B) and the parental aptamer apMNK2F that was completely degraded when incubated with 1 unit of DNAse I.[31] In addition, apMNKQ2 was incubated with human plasma for 6, 16, 48, and 72 h (Figure S3C), and no degradation was observed at the different times tested supporting the very high stability of this aptamer.
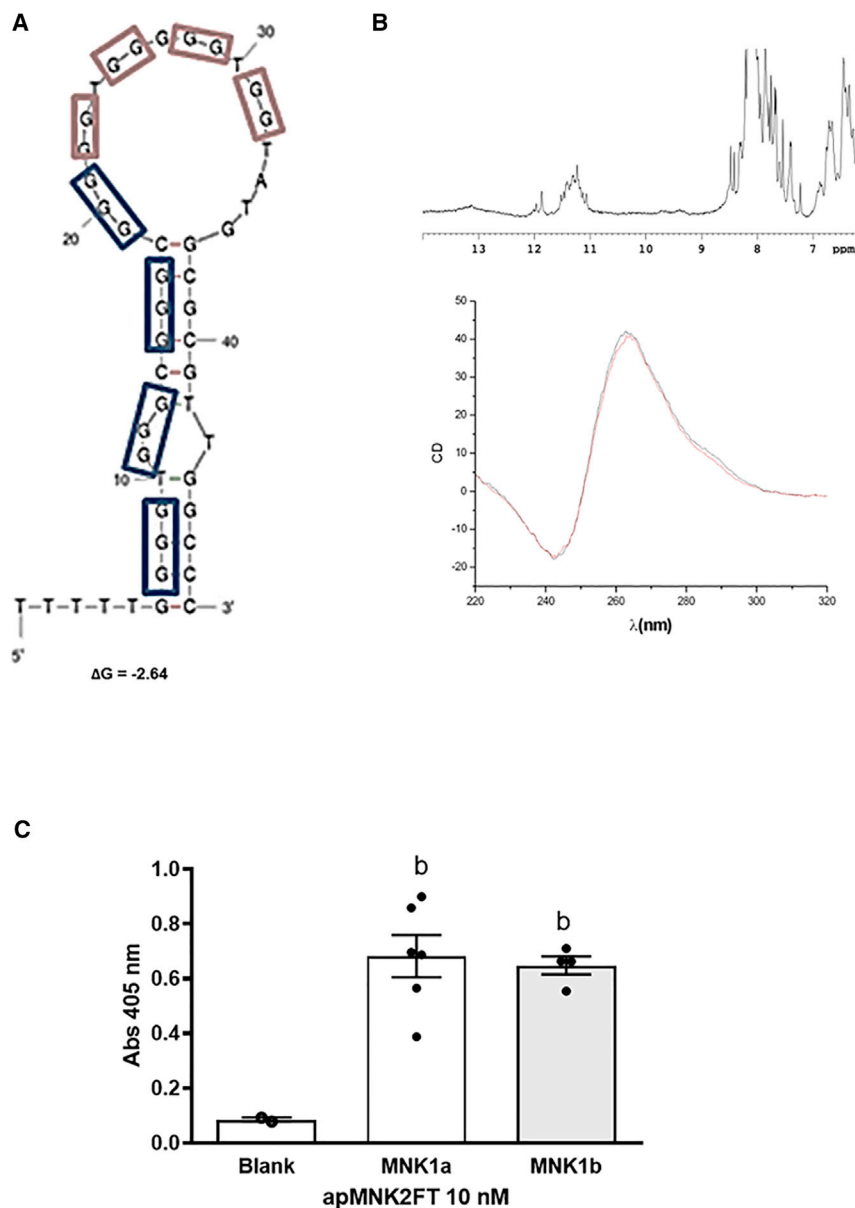
$\Delta G = -2.64$



**Figure 1. Conserved secondary structure and affinity of apMNK2FT**

(A) Graphical representation of the prediction of the secondary and G-quadruplex structures of the truncated aptamer apMNK2FT obtained using mFold and QGRS mapper software. (B) ^{1}H NMR spectra of apMNK2FT at T = 25°C (Top) and CD spectra at 5°C (black) and 25°C (red) (Bottom). Buffer conditions: 10 mM potassium phosphate, pH 7. (C) Binding to MNK1 isoforms by ELONA. Recombinant MNK1a and MNK1b proteins (3 pmol/well) were incubated with 10-nM biotin-conjugated apMNK2FT. The ELONA assay was performed as described in Materials and methods. The bars represent the mean ± standard error of the mean of three independent experiments. [b]p < 0.01, relative to blank.

maximal binding and the dissociation constant (KD) is the concentration of ligand required to reach half-maximal binding. apMNKQ2 was capable of detecting MNK1a and MNK1b proteins in a concentration-dependent manner with KD of 66.13 ± 20.18 and 15.47 ± 2.36 nM, respectively, indicating that the aptamer has much more affinity for MNK1b than MNK1a (more of 4-fold).

In contrast, we have carried out apta-western blot assays using apMNKQ2 conjugated with biotin to confirm the affinity of apMNKQ2 for the two MNK1 isoforms. As shown in Figure 3B, apMNKQ2 is able to recognize the two isoforms of the protein in a similar extent under denaturing conditions; nevertheless, the apMNKQ2 aptamer is able to discriminate significantly between MNK1b and MNK1a under native conditions, confirming the previous result obtained by ELONA assays. These results indicate that the domain that recognizes the aptamer is less accessible in the MNK1a isoform.

In addition, we carried out ELONA assays using recombinant MNK2 and the two MNK-upstream MAPKs, p38MAPK and ERK1. As shown



Altogether, these results reinforce the potential clinical use of apMNKQ2 in the treatment of cancer.
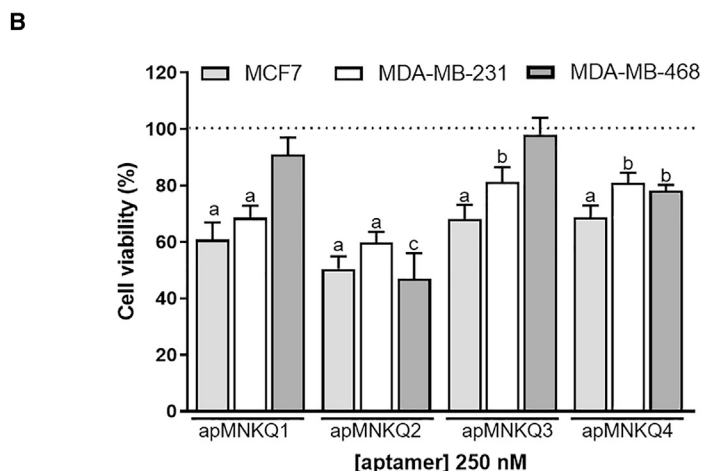
### apMNKQ2 has more affinity for MNK1b than for MNK1a

To study the affinity of apMNKQ2 for both MNK1 isoforms, we made enzyme-linked oligonucleotide assay (ELONA) assays in which GST-MNK1a or GST-MNK1b proteins were incubated with increasing concentrations of biotin-labeled aptamers. A random sequence of 29 nucleotides (GCGGTCGACTTAAATGTCCATCTCAAACT), named p29, was used as a negative control (Figure 3A). The data obtained were analyzed using nonlinear regression showing that respond to a hyperbola whose equation is $y = (x \times B_{max})/(x + KD)$ where $B_{max}$ is the

in Figure 3C, apMNKQ2 did not have an affinity for these kinases, indicating that is specific for MNK1 isoforms.

### apMNKQ2 inhibits cell proliferation and colony formation in breast cancer cells

We first investigated the anti-proliferative effect of the aptamer apMNKQ2 in the three breast cancer cell lines. For this, cells were transfected with the apMNKQ2 or the unspecific p29 aptamer at different concentrations; cell viability was measured after 48 h by MTT reduction. The nonspecific p29 aptamer did not affect cell viability or only slightly (<20%). The apMNKQ2 aptamer did decrease cell viability in the three cell lines having the greatest

**A**

apMNK2FT (48 nt): 5′-TTTT-T**GGGG**T**GGG**C**GGG**C**GGG**-GGT**GGG**GG**T**GG**T**-AT**GG**CGCGTT**GG**CCC-3′
apMNKQ1 (18 nt):          5′-T**GGGG**T**GGG**C**GGG**C**GGG**G-3′
apMNKQ2 (29 nt):          5′-T**GGGG**T**GGG**C**GGG**C**GGG**-GG**T**GGG**GG**T**GG**T-3′
apMNKQ3 (13 nt):              5′-**GGG**T**GG**GG**G**T**GG**T-3′
apMNKQ4 (22 nt):                              5′-G**GGT**GG**T**-AT**GG**CGCGTT**GG**CCC-3′

**B**



Figure 2. Optimized apMNKQs aptamers of apMNK2FT inhibit cell viability in breast cancer cell lines

(A) Sequences of four aptamers obtained from apMNK2FT with predicted G-quadruplex structures. (B) MCF7, MDA-MB-231, and MDA-MB-468 cells were seeded in 96-well plates at a density of $10^4$ cells/well. After 16–24 h, they were transfected with apMNKQ1, apMNKQ2, apMNKQ3, and apMNKQ4 aptamers at 250 nM for 48 h, after which MTT activity assays were performed. Bars represent the mean ± standard error of the mean of three to eight independent experiments. [a]$p < 0.001$, [b]$p < 0.01$, [c]$p < 0.05$ relative to control.

potency against MDA-MB-468 cells and less efficiency against MDA-MB-231 cells. The half maximal inhibitory concentration ($IC_{50}$) values were 42, 144, and 19 nM for MCF7, MDA-MB-231, and MDA-MB-468, respectively (Figure 4A). This effect is not due to necrotic cell death, measured by lactate dehydrogenase (LDH) release assays (Figure S4A). We have also analyzed the number of cells alive by Trypan blue exclusion (Figure S4B) and the cell cycle distribution by propidium iodide staining and flow cytometry (Figure S4C) at concentrations around three times the $IC_{50}$ values (150, 400, and 50 nM for MCF7, MDA-MB-231, and MDA-MB-468, respectively). We observed a significant decrease in the number of alive cells in MCF7 and MDA-MB-468 and an arrest in the phase S of the cycle in MDA-MB-468 cells. However, no significant changes were observed in alive cells and cell cycle distribution in MDA-MB-231 cells (Figures S4B and S4C).

To further determine whether the decrease in cell viability was due to apoptosis induction, cells were transfected with apMNKQ2 or p29 at the concentration indicated above. After 24 h, we analyzed the cleavage of two endogenous substrates of caspase 3, poly (ADP-ribose) polymerase (PARP), and α-spectrin by western blot. apMNKQ2 produced the increase of PARP (Figure 4B) and α-spectrin fragments (Figure S4D) cleaved by caspase 3 in MCF7 and MDA-MB-231 cells, but not in MDA-MB-468 cells.

Next, we analyzed MCL1 and XIAP protein levels, two anti-apoptotic proteins regulated by MNK1.[10,17,32] It is interesting to highlight that apMNKQ2 significantly decreased the levels of MCL1 and XIAP in MCF7 and MDA-MB-231 cells, but not in MDA-MB-468 cells (Figures 4B and 4C).

Finally, we analyzed the effect of apMNKQ2 on the clonogenic capacity of the three breast cancer cell lines; the results showed that the aptamer decreased the number of colonies in all of them, being statistically significant for MCF7 and MDA-MB-231 (Figure 4D).

### apMNKQ2 inhibits migration, invasion, and epithelial-mesenchymal transition in breast cancer cell lines

To evaluate the anti-metastatic effect of apMNKQ2, we performed transwell migration and invasion assays. As shown in Figure 5A, apMNKQ2 was able to inhibit migration in the three cancer cell lines, albeit statistically significantly in MCF7 and MDA-MB-231. In addition, the treatment with the aptamer produced a substantial decrease in invasion in MDA-MB-231 and MDA-MB-468 cells (Figure 5B). In invasion assays, MCF7 cells were not included because in preliminary experiments carried out in our laboratory under control conditions no invasion was observed after 48 h in this cell line (data not shown).

Epithelial-mesenchymal transition (EMT) is defined by the loss of epithelial characteristics and the acquisition of a mesenchymal phenotype. We have analyzed the levels of messenger RNAs (mRNAs) of occludin as epithelial marker and fibroblast-specific protein 1 (FSP1) as mesenchymal marker by quantitative polymerase chain reaction (qPCR). All three cell lines expressed occludin, with the expression being highest in epithelial-type MCF7 cells, whereas FSP1 expression was significantly higher in MDA-MB-231 cells (Figure S5A). The results shown in Figure 5C indicated that apMNKQ2 induced a significant increase in occludin expression in MDA-MB-231 cells. Accordingly, we observed a 1.8-fold increase in occludin protein levels in these cells (Figure S5B). FSP1 expression decreased in MCF7, but did not change in MDA-MB-231 and MDA-MB-468 cells (Figure 5D). These results suggest that apMNKQ2 induces EMT inhibition and, consequently, reduced migration and invasion.

One of the most important inducers of EMT in cancer is transforming growth factor (TGF)-β.[33] TGF-β exerts different effects at different stages of cancer development: it maintains cell proliferation and differentiation in the early stages, but promotes invasion and metastasis
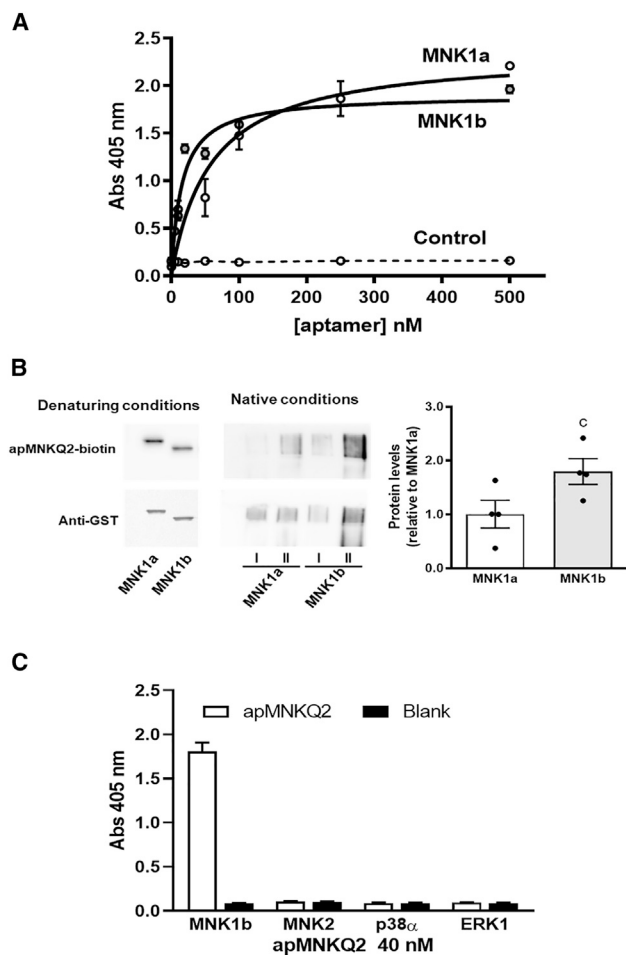
**Figure 3. apMNKQ2 is specific for MNK1 and have higher affinity for MNK1b than for MNK1a**

(A) Analysis of the apMNKQ2 or p29 binding to MNK1b or apMNKQ2 binding to MNK1a was performed by ELONA. GST-MNK1a or GST-MNK1b was plated at 0.2 µg/well (3 pmol/well) and then incubated with apMNKQ2-Bio or p29-Bio at 0–500 nM concentrations. The points represent the mean ± standard error of the mean of three to six independent experiments. (B) Recombinant GST-MNK1a and GST-MNK1b were resolved in SDS-PAGE or native-PAGE and transferred to PVDF membranes. Apta-western blotting was performed with 50 nM apMNKQ2-Bio and streptavidin- horseradish peroxidase (HRP) and developed by ECL. The membranes were reprobed with anti-GST antibodies. The graph at the bottom of the figure represents the quantification of four independent experiments. [C]p < 0.05 relative to MNK1a. (C) The specificity of apMNKQ2 was analyzed by ELONA. Recombinant proteins His-MNK2, p38α, ERK1 and His-MNK1b (5 pmole/well) were incubated with 40 nM apMNK2Q2-Bio or streptavidin-HRP alone (Blank). Bars represent the mean ± standard error of the mean of three independent experiments.

in more advanced stages.[34] To study whether apMNKQ2 affects EMT through the inhibition of TGF-β-induced pathways, we used the immortalized human breast cell line MCF10A, which has been well characterized in TGF-β-induced EMT. MCF10A cells stimulated with TGF-β for 3 or 6 days acquire morphological mesenchymal phenotype (Figure S6A). The decrease in the levels of the epithelial marker E-cadherin and the increase in the mesenchymal marker

N-cadherin can be observed after 3 days of treatment (Figure S6B). In addition, the levels of three transcription factors that play a key role in EMT; ZEB1, Slug, and Snail are also increased (Figure S6B). Then, MCF10A cells were transfected with apMNKQ2 (100 nM) and treated or not with TGF-β. After 48 h of treatment, transwell migration and invasion assays were performed. As shown in Figures 6A and 6B, apMNKQ2 significantly inhibited TGF-β-induced migration and invasion, while it did not affect untreated MCF10A. In addition, a significant decrease in zymography-analyzed MMP-2 activity was observed in both untreated and TGF-β-treated MCF10A cells transfected with apMNKQ2 (Figures 6C and S7A). In agreement with these results, apMNKQ2 produced a decrease in N-cadherin levels in both untreated and TGF-β-treated cells, but, surprisingly, a decrease in E-cadherin levels can be observed (Figures 6D and S7A). Finally, the levels of ZEB1, Slug and Snail were also analyzed by western blot. The aptamer apMNKQ2 reduced the ZEB1 and Slug levels, in both untreated and TGF-β-treated cells, whereas Snail levels increased after apMNKQ2 treatment (Figures 6D and S7A). An analysis of mRNA levels indicated that the decrease in ZEB1 and Slug is not mediated by transcription downregulation, whereas, probably, the increase of Snail is produced at the transcription level (Figure S7B). Similarly, apMNKQ2 induced the decrease in ZEB1 and an increase in snail protein levels, but did not affect Slug protein levels in MDA-MB-231 cells, while the levels of the mRNAs increased after apMNKQ2 treatment (Figure S7C).

## apMNKQ2 decreases the levels of MNK1 isoforms and eIF4EP in the MDA-MB-231 breast cancer cell line

In our previous work, using the parental aptamer against MNK1, apMNK2F, we could not find an effect of the aptamer on eIF4E phosphorylation.[31] Here, we have analyzed whether the optimized aptamer apMNKQ2 induced eIF4E dephosphorylation. In these assays, MDA-MB-231 cells were transfected with apMKQ2 or with p29 control aptamer at 400 nM. After 24 h of transfection, protein levels were analyzed by western blot using specific antibodies. Our results showed that, at this time, apMNKQ2 induced a significant decrease in eIF4E phosphorylation (Figure 7A). In addition, the levels of both MNK1a and MNK1b isoforms, but not MNK2, were significantly decreased (Figure 7A). This decrease was not due to a decrease in mRNA levels (Figure 7B).

## apMNKQ2 reduces tumor growth and metastasis number *in vivo*

To evaluate the potential therapeutic activity of apMNKQ2, an orthotopic xenograft mouse model of MDA-MB-231 cells was used. The results showed that 1.8 mg/kg apMNKQ2 decreased the relative tumor volume (RTV) significantly from day 7 of treatment reaching a tumor growth inhibition (TGI) of 26% at the end of treatment (18 days) (Figure 8A). Furthermore, there were no difference in weight between treated and untreated mice, suggesting that apMNKQ2 is safe at the dose administered (Figure 8B). The proliferation index, measured by immunohistochemistry with the proliferating cell nuclear antigen (PCNA) antibody, confirmed a significant 33% reduction in tumors from apMNKQ2-treated mice relative to control mice (Figure 8C). In addition, the PARP cleavage increased significantly in the tumors from apMNKQ2-treated mice, indicating apoptosis induction
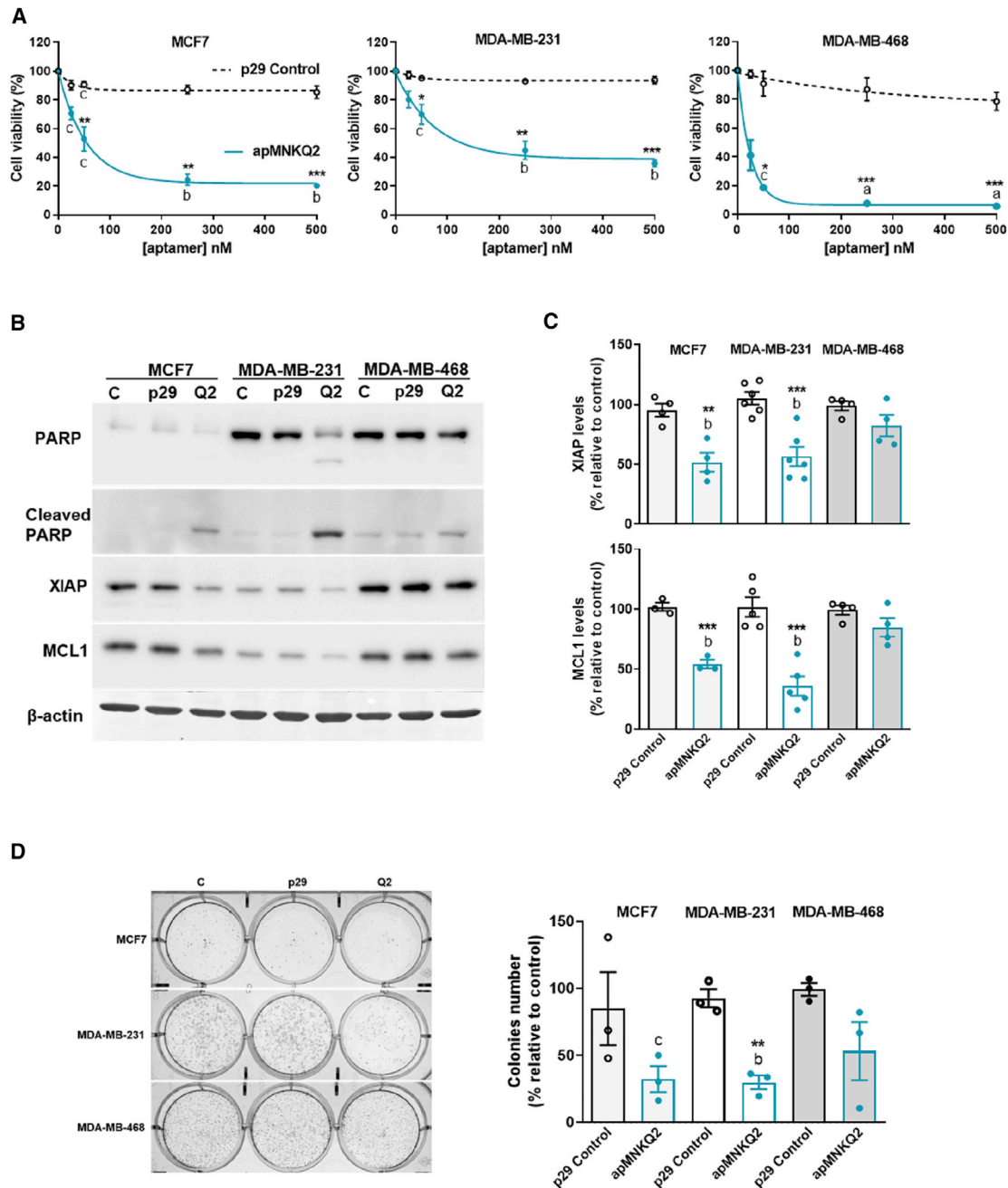
**Figure 4. apMNKQ2 inhibits cell viability, induces apoptosis by downregulating anti-apoptotic proteins, and inhibits colony formation in breast cancer cell lines**

(A) MCF7, MDA-MB-231, and MDA-MB-468 cells were seeded in 96-well plates at a density of $10^4$ cells/well. After 16–24 h, they were transfected with apMNKQ2 (blue line) or the control p29 (black line) at different concentrations (0–500 nM) for 48 h, and then MTT assay was performed. Bars represent the mean ± standard error of the mean of three independent experiments. (B) Lysates (20–30 μg) were subjected to SDS-PAGE at 10% for total PARP, cleaved PARP, MCL1, and XIAP and western blot was performed using specific antibodies (see Table S1). Actin was used as a control for homogeneity of loading. A representative blot is shown. (C) Quantification of bands of XIAP and MCL1 from western blot (B) was normalized with respect to actin and expressed as the percentage relative to the value in control cells. Values represent the mean ± standard error of the mean of three to six different experiments. (D) Cells transfected with apMNKQ2 or p29 at 3 times the $IC_{50}$ were seed at $1 \times 10^3$ cells/well in six-well plates. After 8–9 days, colonies were fixed, stained, and counted. Bars represent mean ± standard error of the mean of three independent experiments. [a]p < 0.001, [b]p < 0.01, [c]p<0.05 relative to control cells; ***p < 0.001, **p < 0.01, *p < 0.05 relative to p29 control. See also Figure S4.
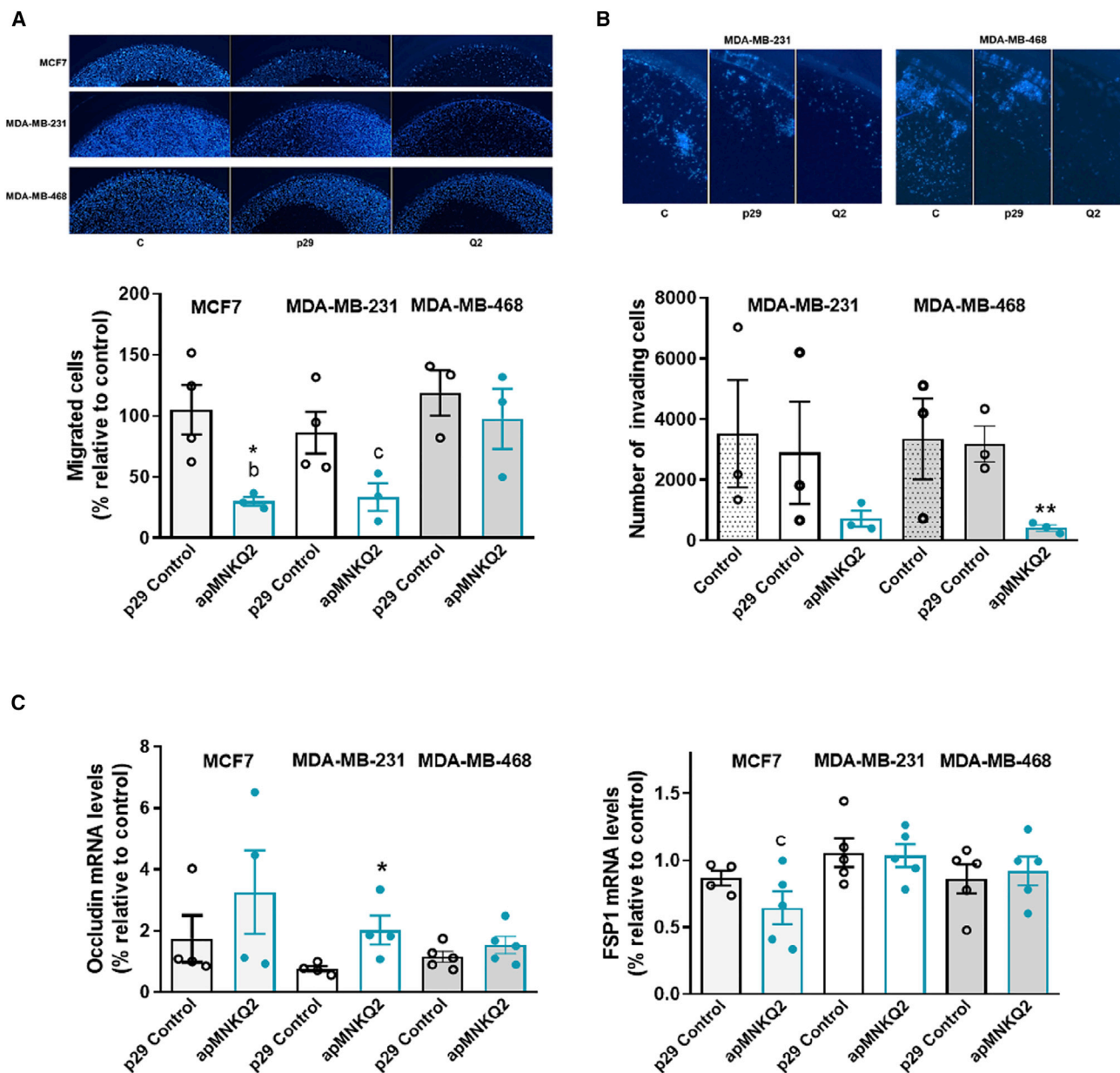
**Figure 5. apMNKQ2 inhibits migration, invasion, and EMT in breast cancer cell lines**

Cells transfected with apMNKQ2 or p29 at 3 times the $IC_{50}$ were maintained in serum-deprived medium for 16 h, then collected, counted and seeded ($4 \times 10^4$ cells) for transwell assay without or with matrigel to measure migration (A) and invasion rate (B), respectively. Representative images are shown at the top of the figures. (A) Data are expressed as the percentage relative to the value of control cells and (B) the number invading cells and represent the mean ± standard error of the mean of three to four different experiments. (C) Quantitative reverse transcriptase PCR analysis of occludin and FSP1 (normalized with respect to actin expression) was performed as described in the Materials and Methods section. Bars represent the mean ± standard error of the mean of three to five different experiments. [b]$p < 0.01$, [c]$p < 0.05$ relative to control cells; **$p < 0.01$, *$p < 0.05$ relative to p29 control. See also Figure S5.

(Figure 8D). To validate whether the tumor reduction is specific to apMNKQ2 treatment, we measured MCL1 levels and occludin mRNA levels, two of the most significant changes observed when treating MDA-MB-231 cells *in vitro* (Figures 4C and 5C). There was a significant decrease in MCL1 levels (Figure 8E) and an increase in occludin mRNA levels (Figure 8F) in agreement with the results previously obtained *in vitro*. Occludin protein levels also increased, but were not statistically significant (Figure 8G). We repeated this assay with very similar results. As shown in Figure S8A, TGI was 27.5% after 18 days ($p < 0.05$) of treatment with apMNKQ2 2 mg/kg and 29.1% at
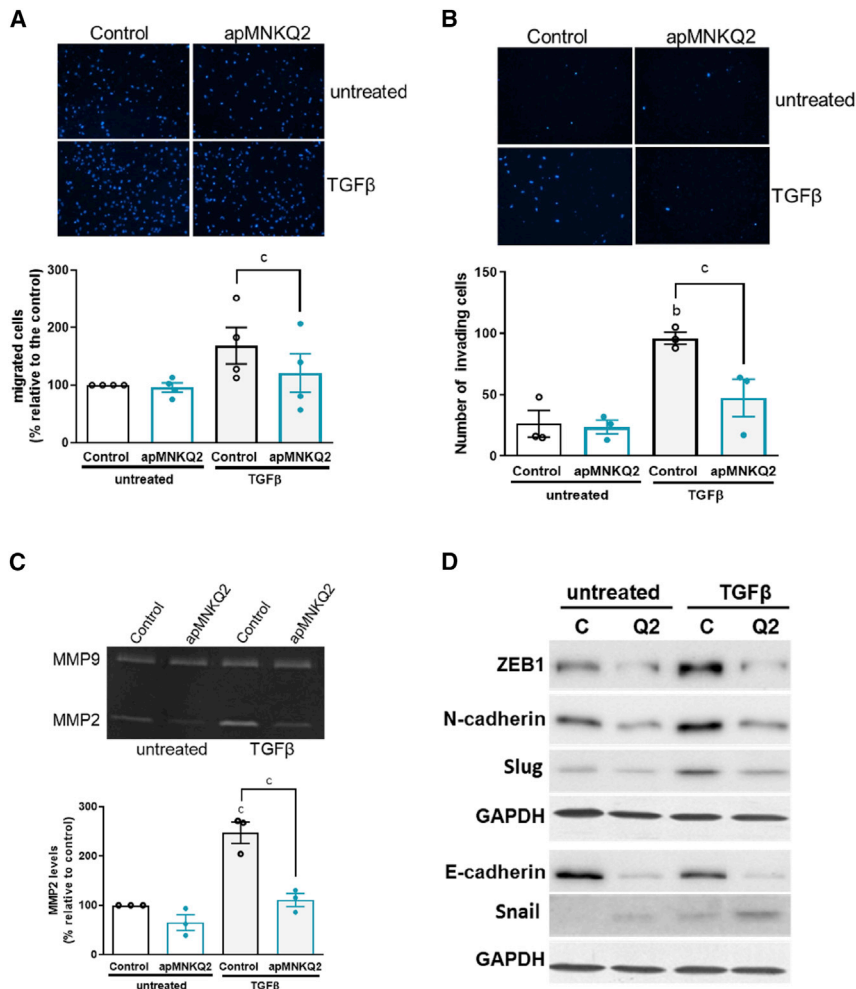
**Figure 6. apMNKQ2 inhibits TGF-β-induced EMT in MCF10A cells**

MCF10A cells transfected with apMNKQ2 and treated with 5 ng/mL TGF-β in medium containing 0.5% horse serum. After 48 h, cells were harvested, counted and seeded ($6 \times 10^4$ cells) for transwell assay without or with matrigel to measure migration (A) and invasion rate (B), respectively. (A) Data are expressed as the percentage relative to the value in control cells (not transfected and not treated with TGF-β) and (B) the number of invading cells and represent the mean ± standard error of the mean of three to four different experiments. (C) Zymograms are performed as described in the Materials and Methods section. Quantification of bands is expressed as the percentage relative to the value in control cells and represent the mean ± standard error of the mean of three different experiments. (D) Levels of epithelial/mesenchymal markers and transcription factors involved in EMT were analyzed by western blot using specific antibodies (see Table S1). Glyceraldehyde 3-phosphate dehydrogenase (GAPDH) was used as a control for homogeneity of loading. Representative blots are shown. $^b p < 0.01$, $^c p < 0.05$ relative to control. See also Figures S6 and S7.

apMNKQ2 did not decrease the RTV at any time point during treatment (18 days) (Figure S9D). Furthermore, there were no differences in weight between the treated and untreated mice, which also suggests that apMNKQ2 was safe at the dose administered in a syngeneic model (Figure S9E). The number and size of metastases in the lung were analyzed at the end of treatment using the inverse tincture method with Chinese ink. Metastases were separated according to their size down to 0.5, 1, 2, and more than 2 mm. As shown in Figure S9F, apMNKQ2 produced a 50% decrease in the total number of metastases (p = 0.06), and reduced the size of metastases, with significantly fewer metastases around 2 mm.

the end of treatment (28 days). In addition, one group of animals was treated with everolimus 2 mg/kg, a drug used clinically for the treatment of breast cancer, reaching a TGI of 47.5% at the end of treatment (Figure S8A). As in the previous assay, an increase in occludin mRNA levels (Figure S8B) and a decrease in MCL1 protein levels (Figure S8C) were also observed. An attempt was made to improve the efficacy of apMNKQ2 by increasing the doses; however, 4 mg/kg exceeds the maximum amount of nucleic acids that can be conjugated with *in vivo* Jet-Pei, being toxic to the animals (results not shown).

To also evaluate the potential anti-metastatic effect of apMNKQ2, we used a spontaneous metastasis model in BALBc mice bearing orthotopic 4T1 breast tumors. First, we studied the effect of apMNKQ2 on proliferation, migration, and invasion in this mouse breast cancer cell line. Surprisingly, apMNKQ2 did not produce a significant decrease in cell viability in 4T1 cells at the concentrations used (up to 1 µM) (Figure S9A), but was able to inhibit migration (as measured by scratch wound-healing and transwell migration assays) and invasion (Figures S9B and S9C). These results showed that 3.6 mg/kg

Altogether, these results indicate the potential use of apMNKQ2 as an anti-tumor and anti-metastatic drug in breast cancer.

## DISCUSSION

Despite advances in prevention, diagnosis, and treatment and, therefore, the consequent increase in survival, breast cancer remains a complex and heterogeneous disease that, in many cases, has no cure and that leaves an average survival time of 18–24 months, depending on the extent of the tumor and its histopathological and molecular profiles.

In a previous article, we described that the aptamer apMNK2F, an aptamer selected in our laboratory against the MNK1b protein, was able to inhibit proliferation, migration, and colony formation in MDA-MB-231 breast cancer cells.[31] Furthermore, by in silico studies, we
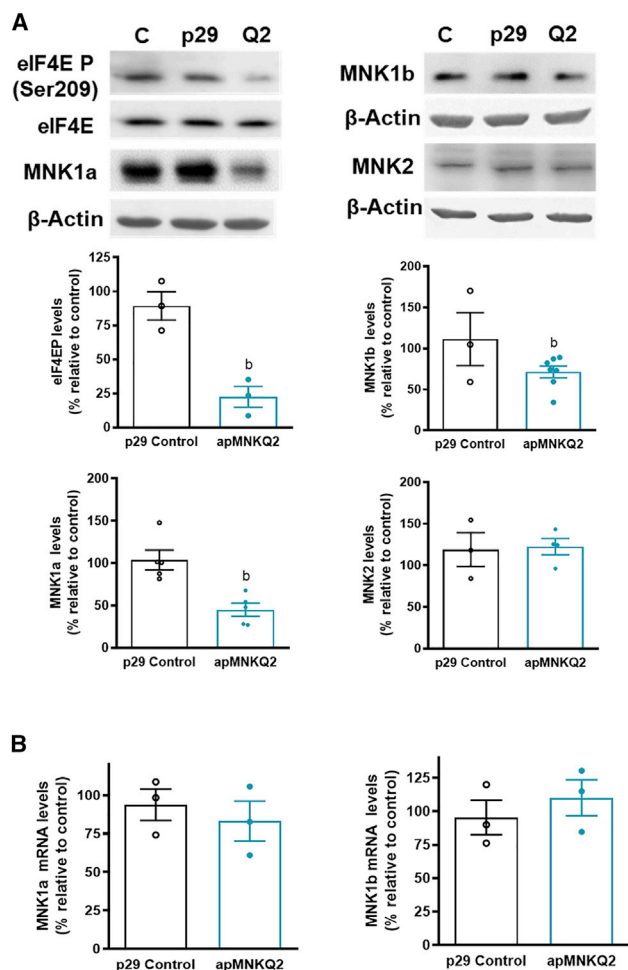
**Figure 7. apMNKQ2 decreases the levels of MNK1 isoforms and eIF4EP in MDA-MB-231 breast cancer cell line**

Cell lysates or total RNA were obtained from MDA-MB-231 transfected with apMNKQ2 or control p29 aptamer at 400 nM during 24 h as described in the Materials and Methods section. (A) Lysates (20 μg) were subjected to SDS-PAGE at 12% and western blotting was performed using specific antibodies (see Table S1). Actin was used as a control for homogeneity of loading. Quantification of the bands was normalized with respect to actin, and expressed as the percentage relative to the value in untreated control cells. Values represent the mean ± standard error of the mean of three to seven different experiments. Representative blots are shown on the left of the figure. [b]$p < 0.01$ relative to control. (B) Quantitative reverse transcriptase PCR analysis of MNK1a and MNK1b (normalized with respect to actin expression) was performed as described in the Materials and Methods section. Bars represent the mean ± standard error of the mean of three different experiments.

demonstrated that this aptamer could have the ability to form two G-quadruplex structures. G-quadruplex-forming aptamers have been described to have important advantages over unstructured sequences in that they are not immunogenic, are thermodynamically and chemically stable, and show both increased resistance to various serum nucleases and increased cellular uptake.[35] In contrast, reducing the size of the aptamer allows better accessibility to its target and a better distribution inside the cell, decreasing production costs. In

this regard, we first set out to optimize the apMNK2F aptamer by removing regions of the sequence that did not seem to be involved in the formation of the G-quadruplex structure and to determine whether this optimization would result in a smaller aptamer that retained its activity. The new shorter aptamer, apMNK2FT, retains the G-quadruplex structures and maintains its ability to bind MNK1 isoforms with high affinity. However, it is much less effective than apMNK2F in inhibiting processes characteristic of tumor cells, such as proliferation or migration, but not colony formation, in the breast cancer cell line MDA-MB-231. After a detailed analysis of the aptamer apMNK2FT using QGRS Mapper software four different sequences (apMNKQ1, apMNKQ2, apMNKQ3, and apMNKQ4) with the ability to form G-quadruplex structures were predicted (Figure 2A). Among them, the selected candidate, apMNKQ2, with only 29 nts, inhibits MTT activity in breast cancer cells and is resistant to degradation by DNAse I and by enzymes presented in human plasma supporting that G-quadruplex structures confer high stability.

One of the properties sought when identifying new anti-tumor drugs is their ability to inhibit processes involved in the development of the tumor itself, such as cell proliferation, apoptosis, and clonogenic activity. We have shown that apMNKQ2 is able to decrease cell viability in three human breast cancer cell lines (MCF7, MDA-MB-231, and MDA-MB-468) but not in 4T1 mouse breast cancer cell line. Although most MNK inhibitors have an anti-proliferative effect, in some cases it is not affected. Thus, the MNK-7g inhibitor does not affect the distribution of MDA-MB-231 cells in the cell cycle, indicating that it does not affect cell viability. However, it is able to exert its action by inhibiting migration, suggesting that MNK may be affecting metastasis-related processes.[23]

Metastasis is a complex process that requires multiple events, including the EMT of epithelial cancer cells, induction of angiogenesis, and intravasation and extravasation of cancer cells, for the cells to regain epithelial features (MET) and eventually form a new colony in the appropriate distant microenvironment. There is much evidence that MNKs play an important role in metastasis-related events.[36] For example, the inhibition of MNKs decreases protein expression of the EMT-activating transcription factor ZEB1, leading to the inhibition of EMT and reduction of migration and invasion of pancreatic cancer cells.[37] In this work, we have demonstrated that apMNKQ2 is able to inhibit migration and invasion both in breast cancer cells and in an *in vivo* model. In contrast, apMNKQ2 acts by regulating EMT, affecting the expression of the main transcription factors involved in this process. EMT transcription factors are known to regulate each other in complex patterns that have not been established yet and that depend on tumor type and tissue context.[38] In our TGF-β model, apMNKQ2-induced reduction of ZEB1 and Slug expression could lead to an increase of Snail at the mRNA and protein levels. Similar results were described in oral cancer cells and hepatocellular carcinoma cells using Slug and ZEB1 small interfering RNAs (siRNAs), respectively.[39,40] Since Snail acts as a direct repressor of E-cadherin,[41] the observed Snail overexpression may be associated with a low E-cadherin expression. However, apMNKQ2 inhibits
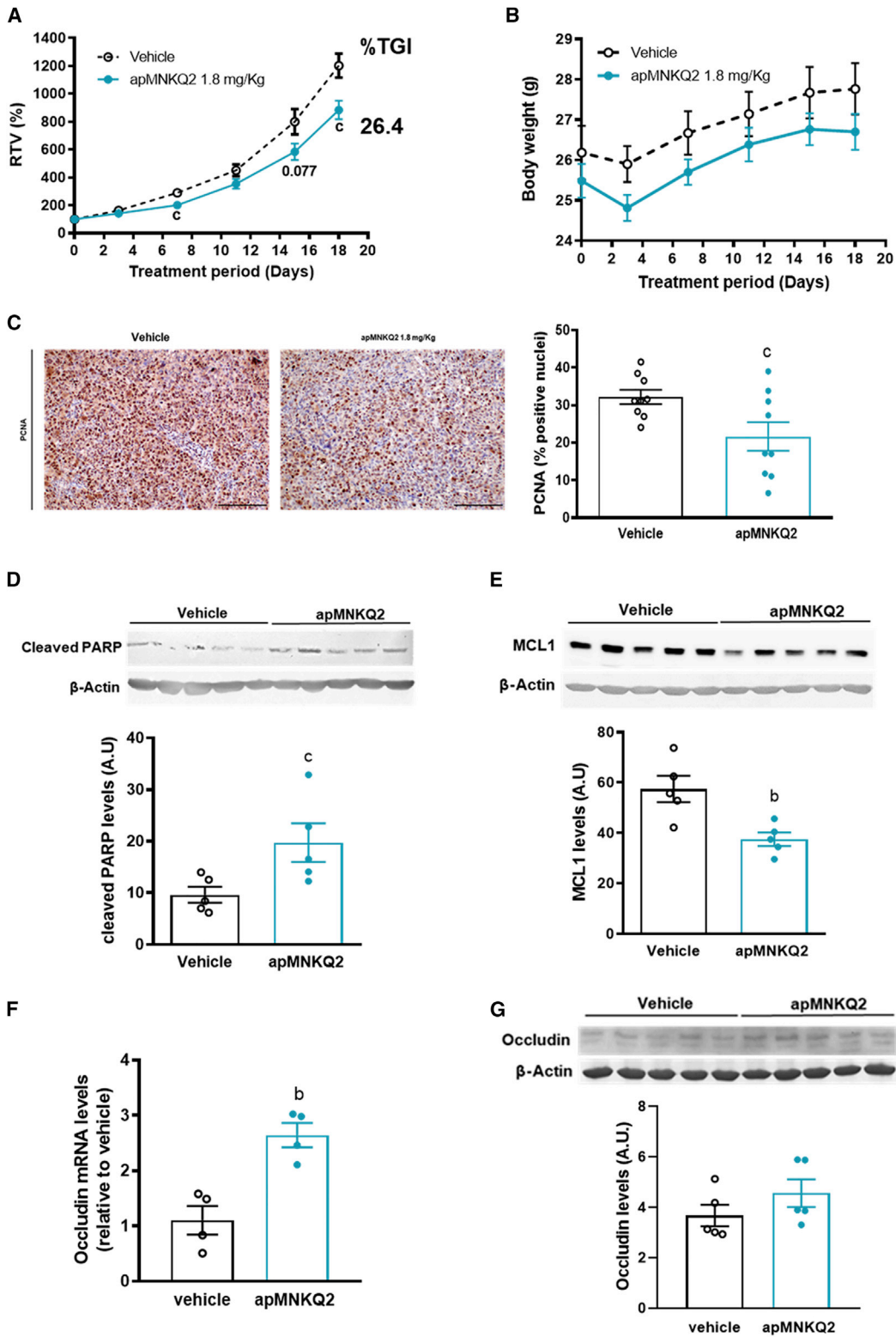
TGF-β-induced migration in breast cancer cells, as it is able to reduce N-cadherin levels. Consistent with our findings, N-cadherin knock down MCF10A cells have lower cell motility in the presence of TGF-β,[42] while E-cadherin depletion in MCF10A also results in slow migration.[43] In addition, there is a decrease in MMP2 activity that was upregulated by TGF-β, which may be related with the inhibition of invasiveness.

The most widely used traditional inhibitors of MNKs (CGP57380 and cercosporamide) had low selectivity and efficacy, exerting off-target effects.[44–46] For this reason, efforts have been made to identify inhibitors that can be more specific. Most of the newly designed and synthesized MNK inhibitors present $IC_{50}$ values in the micromolar or high nanomolar range and recognize both MNK1 and MNK2.[1,23,47] This is probably because they have been obtained by searching for molecules that block the kinase activity, specifically the catalytic site of the enzyme, which is highly conserved in different kinases. Instead, a new family of inhibitors that acts as MNK "degraders" is being developed.[48–50] To our knowledge, apMNKQ2 is the first specific MNK1 inhibitor developed and is able to significantly and specifically downregulate MNK1 isoforms through a mechanism that remains to be elucidated.

We have presented evidence implying that the aptamer apMNKQ2, developed against MNK1 kinase, is a potential therapeutic agent for the treatment of breast cancer and possibly other tumors in which MNK1 plays a relevant role.[9] Additional efforts are currently underway to find the best delivery method, and to carry out in vivo studies that allow us to determine the optimal effective dose and then to perform the corresponding pharmacodynamics and pharmacokinetic studies.

## MATERIALS AND METHODS
### Expression and purification of recombinant proteins
GST-tagged human MNK1a and MNK1b were subcloned into the BamHI and NotI sites of pGEX-4T3 and expressed in Escherichia coli Rosetta cells. Proteins were purified with glutathione-Sepharose (GenScript, Piscataway, NJ) according to the manufacturer's instructions. Briefly, expression was induced with 1 mM IPTG for 2 h at 25°C. Cells were suspended in buffer containing 5 mM sodium phosphate, 150 mM NaCl, 1 mM EDTA (pH 7.4), and 1 mg/mL lysozyme, and incubated on ice for 30 min. Afterward, 0.5% Triton X-100 was added and bacteria were subjected to sonication. Cell debris was removed by centrifugation, and the supernatant was incubated with glutathione-Sepharose equilibrated in the same buffer by rocking

for 2 h at 4°C. Finally, after extensive washes with the same buffer, the proteins were eluted with 10 mM glutathione in 50 mM Tris-HCl (pH 8).

His-MNK1b, cloned as described in[31] was purified by affinity chromatography by ProAlt (Protein Alternatives S.L., Madrid, Spain).

### ELONA
Recombinant proteins (200 ng) diluted in coating buffer (SeraCare, Milford, MA) were incubated in a 96-well microtiter plate (NUNC, Rochester, NY) overnight at 4°C. Then, the plate was blocked using 5% bovine serum albumin in phosphate-buffered saline (PBS) and incubated 1 h at room temperature, and subsequently washed four times in selection buffer (20 mM Tris-HCl pH 7.4, 150 mM NaCl, 1 mM $MgCl_2$, 5 mM KCl). The modified apMNK2F aptamers (apMNK2FT and apMNKQ2), conjugated with biotin, were diluted in selection buffer at the concentrations indicated in the figures, denatured for 10 min at 95°C and cooled for 10 min on ice. Next, 100 μL of the diluted aptamers were added to each well, the plate was incubated at 37°C for 1 h and washed four times with selection buffer to remove unbound ssDNA. Afterward, 100 μL of a 1/1,000 dilution of horseradish peroxidase-conjugated streptavidin (GE Healthcare, Madrid, Spain) were added to the individual wells. After 1 h incubation at 37°C on a shaking platform, the plates were washed four times and developed using ABTS solution (Roche, Madrid, Spain) according to the manufacturer's instructions. OD 405 nm values were determined using a SpectraFluor microplate reader (TECAN, Barcelona, Spain).

### Secondary structure prediction
Aptamer secondary structure prediction was obtained using mFold software (http://mfold.rna.albany.edu/?q=mfold/DNA-Folding-Form) at 37°C, 150 mM [Na⁺] and 1 mM [Mg⁺⁺] (selection buffer conditions) and QGRS Mapper (https://bioinformatics.ramapo.edu/QGRS/index.php), a web-based server for predicting G-quadruplexes in nucleotide sequence.

### NMR and CD
The aptamers were resuspended in $H_2O/D_2O$ 9:1 in 10 mM potassium phosphate buffer, pH 7, [DNA] ∼ 100 μM. NMR spectra were acquired in Bruker Avance spectrometer operating at 600 MHz, and processed with Topspin software. Water suppression was achieved by including a WATERGATE module in the pulse sequence

**Figure 8. apMNKQ2 reduces tumor growth in vivo**

(A) Growth of orthotropic tumors generated in NOD-SCID mice by injection of MDA-MB-231 cells into the mammary fat pad. Animals were treated with vehicle (selection buffer: in vivo-jetPEI) or apMNKQ2:in vivo-jetPEI (1.8 mg/kg) 3 times per week. Data are expressed as the RTV and represent the mean ± standard error of the mean of nine animals. TGI, calculated as described in the Materials and Methods section, is indicated at the right of the line. (B) Body weight was measured twice a week. Values represent the mean ± standard error of the mean of nine animals. (C) PCNA-positive cells were measured by immunohistochemistry using an anti-PCNA antibody as described in Materials and Methods section. Scale bar, 100 μm. Data are expressed as the percentage of positive nuclei and represent mean ± standard error of the mean of nine animals. Blots and corresponding quantification of cleaved PARP (D), MCL1 (E), and occludin (G) are shown. Western blotting was performed using specific antibodies (see Table S1) as described in the Materials and Methods section. Actin was used as a control for the homogeneity of loading. Data are expressed in arbitrary units (A.U.) and represent the mean ± standard error of the mean of five animals. (F) Quantitative reverse transcriptase PCR analysis of occluding (normalized with respect to actin expression) was performed as described in the Materials and Methods section. Bars represent mean ± standard error of the mean of four animals. $^{b}p < 0.01$, $^{c}p < 0.05$ relative to control. See also Figure S8.

prior to acquisition. CD spectra were recorded on a Jasco J-815 spectropolarimeter fitted with a thermostatted cell holder. Spectra were recorded at a DNA concentration of 50 µM and under the same buffer condition as the NMR experiments.

### Aptamer stability assays

apMNKQ2 aptamer (1 µg) was incubated with 0.25, 0.5, or 1 U of DNAse I (Thermo Fisher Scientific, Waltham, MA) for 5 min at 37°C. Subsequently, the reaction was stopped by adding 1 µL EDTA 50 nM and heating the samples at 65°C for 10 min. The digested aptamer apMNKQ2 was resolved on a chip Experion DNA1K Analysis f Kit (BioRad, Hercules, CA), following the manufacturer's instructions.

In plasma, 2.4 µg apMNKQ2 plus 16 µL of human plasma was incubated at 37°C for up to 72 h. Aliquots of the mixture were removed at 0, 6, 24, 48, and 72 h and heated for 10 min at 65°C to inhibit the activity of nucleases present in the plasma, and cooled on ice for 10 min. They were kept at −20°C until all aliquots were obtained, and finally loaded onto a chip Experion DNA 1K Analysis Kit.

### Cell culture and protein and RNA extraction

MCF7 and MDA-MB-231 cells, last authenticated in May 2019 and June 2021, respectively, using the GenePrint 10 System, were maintained in Dulbecco's modified Eagle's medium (DMEM)/Ham F-12 medium (PAA, Pasching, Austria) (mixed 1:1) with 10% fetal calf serum (Gibco, Grand Island, NY) and 100 U/mL penicillin, 100 µg/mL streptomycin, and 25 µg/mL amphotericin (Sigma, St. Luois, MO) in a humidified incubator with 5% $CO_2$/95% air at 37°C. MDA-MB-468 cells, last authenticated in May 2019 using the GenePrint 10 System, were maintained in RPMI medium (PAA, Pasching, Austria) with 10% fetal calf serum (Gibco) and 100 U/mL penicillin, 100 µg/mL streptomycin, and 25 µg/mL amphotericin (Sigma) in a humidifed incubator with 5% $CO_2$/95% air at 37°C. MCF10A cells (purchased from ATCC, Manassas, VA) were maintained in DMEM/Ham F-12 medium (PAA, Pasching, Austria) supplemented with 10 µg/mL insulin (Sigma), 20 ng/mL epidermal growth factor (Sigma-Aldrich), 0.5 µg/mL hydrocortisone (Sigma), 5% horse serum (Gibco), 100 U/mL penicillin, 100 µg/mL streptomycin, and 25 µg/mL amphotericin (Sigma) in an incubator with 5% $CO_2$/95% air at 37°C. To obtain lysates, cells were washed once with cold buffer A \(20 mM Tris-HCl pH 7.6, 1 mM dithiothreitol, 1 mM ethylenediaminetetra-acetic acid, 1 mM phenylmethylsulfonyl fluoride, 1 mM benzamidine, 10 mM sodium molybdate, 10 mM sodium β-glycerophosphate, 1 mM sodium orthovanadate, 120 mM potassium chloride, 10 µg/mL anti-pain, 1 µg/mL pepstatin A and leupeptin), and were mechanically harvested and lysed in the same buffer containing 1% Triton X-100 (volume ratio 1:2) and centrifuged at 12,000 g for 10 min. For tissues, tumors were thawed, weighed, and protein lysates were obtained as described above. Subsequently, protein concentration was determined using the BCA Kit (Thermo Fisher Scientific) and supernatants were aliquoted and stored at −80°C until use.

Total RNA from cells and tumor tissues were lysed and homogenized in NucleoZOL (Macherey-Nagel, Düren, Germany) following the manufacturer's protocol. The RNA pellet was resuspended in 50 µL of Rnase-free water, treated with 1 µL of DNAse I (Fermentas, Waltham, MA), quantified, and stored at −80°C.

### Western blot and apta-western assays

Cell lysates (20–30 µg) were resolved on 12%, 15%, or 10% sodium dodecyl sulphate-polyacrylamide gel electrophoresis (SDS-PAGE) under the conditions indicated in figure legends, and transferred to polyvinylidene fluoride (PVDF) membranes. The membranes were incubated with monoclonal or polyclonal antibodies overnight at 4°C. After washing, the membranes were incubated with the corresponding peroxidase-conjugated secondary antibody (GE Healthcare) for 1 h at room temperature and developed with enhanced chemiluminescence's kits (GE Healthcare) or Clarity Western ECL Substrate (BioRad). PageRuler Plus Prestained Protein Ladder (Thermo Fisher Scientific) was used in all the experiments. The β-actin antibody (Sigma) was used as a control to monitor the homogeneity of loading. Antibodies used in this study are listed in Table S1.

For apta-western assays, 100 ng purified MNK1 proteins were resolved on gel electrophoresis under denaturing (SDS-PAGE) or native (PAGE, neither SDS nor β-mercaptoethanol were used) conditions and transferred to PVDF membranes. The membranes were incubated with 50 nM biotin-conjugated apMNKQ2. After washing, the membranes were incubated with streptavidin-peroxidase 1:5,000 (GE Healthcare) and developed as above.

### MTT and LDH assays

MCF7, MDA-MB-231, or MDA-MB-468 cells were seeded at $10^4$ cells/well in 96-well plates. After 16–24 h, aptamers or unspecific p29 ssDNA were transfected at the concentrations indicated in the figure legends using Lipofectamine 2000 (Invitrogen, Waltham, MA) following manufacturer's instructions for siRNA transfection. After 48 h, the medium was removed to add 100 µL MTT (1 mg/mL in culture medium) to each well, and the plates were incubated 3 h at 37°C. Then, 100 µL/well of lysis buffer (10% SDS and 10 mM HCl) was added and, after 24 h of incubation, the absorbance was read at 540 nm on a SpectraFluor microplate reader (TECAN, Männedorf, Switzerland).

To perform cell death (LDH) assays, 48 h after aptamer transfection, supernatants were collected for mixing with the cytotoxicity detection kit (LDH) reagent (Roche), following the manufacturer's protocol. The reaction was incubated for 30 min at room temperature, and stopped by adding 1 M HCl. Finally, solubilized formazan was measured in an Infinite F200 spectrophotometer (TECAN, Männedorf, Switzerland) at 490 nm. To calculate the percentage of cytotoxicity, two controls were included: supernatants of untreated cells ($LDH_{low}$) and of lysate cells ($LDH_{high}$) with 0.2% Triton X-100. Finally, the results were expressed as cytotoxicity (%) = ($LDH_{treated}$ − $LDH_{low}$)/($LDH_{high}$ − $LDH_{low}$) × 100, for each experimental point with respect to the control.

**Trypan blue exclusion test of cell viability**

To determine the number of viable cells after aptamer transfection, cells were collected from vials or culture plates suspended in their corresponding medium. Aliquots of 40 μL cells mixed with 10 μL trypan blue were counted using a TC20 counter (BioRad), with cells excluding the dye being considered live.

**Flow cytometric analysis of cell cycle**

Twenty-four hours after transfection, the cells were harvested and fixed in cold 70% ethanol for 30 min at $-20°C$. Afterward, cells were washed twice with ice-cold PBS and incubated with 50 μg/mL propidium iodide (Sigma) plus 100 μg/mL RNAse A (Sigma) for 1 h at 37°C in darkness. The cell cycle was analyzed by flow cytometry (FACScalibur, BD Biosciences, Franklin Lakes, NJ) using selective gating to exclude cell doublets. Cytometry data were analyzed using Flowing software 2.5.1. (Turku Bioscience, Turku, Finland).

**Colony-forming assays**

After 16–24 h, transfected cells as described above were collected and alive cells were counted by trypan blue exclusion assay (Sigma) using TC20 counter (BioRad) and seeded at $1 \times 10^3$ or $5 \times 10^3$ cells/well in six-well plates for MCF7 and MDA-MB-231 or MDA-MB-468 respectively. Approximately 12–16 days later, colonies were fixed, stained for 30 min with 0.02% Giemsa (Sigma), and counted with an eCount Colony Counter Pen (Heathrow Scientific, Vernon Hills, IL) and a magnifying glass ($\times 1.75$) (Bel-Art Scienceware, Wayne, NJ).

**Scratch wound-healing assays**

MDA-MB-231 cells were plated in six -well plates at $5 \times 10^5$ cells/well in 2 mL growth medium. After 24 h, the cells were transfected with the aptamer at the concentration indicated in the legends, and treated with 1 μM mitomycin C for 2 h to ensure that the wounds were filled due to cell migration and not by cell proliferation. Subsequently, the monolayer was scraped with a P-200 pipette tip, washed with medium to remove floating cells, and photographed with an Olympus IX70 (time 0). The plates were then incubated at 37°C and images were taken after 24 h. Wound area was measured using ImageJ software and calculated as the percentage of closed wound.

**Migration and invasion assays**

Migration and invasion assays were carried out using transwell insert chambers (Corning, Corning, NY). For the migration assay, cells transfected as described above were harvested after 16 h of serum deprivation, collected, counted, and $4 \times 10^4$ cells were plated in the upper chamber in serum-free medium. Complete medium (10% FBS) was added to the lower chamber as chemoattractant. After 24 h, medium was removed from the top and bottom of the wells; cells in the insert were fixed with 4% formaldehyde for 2 min, followed by 20 min with 100% methanol. Cells were stained with 30 μM Hoechst 33342 for 15 min, protected from light, washed twice with PBS and cells on the top were removed with a cotton stick. At least five photographs were acquired for each sample using a fluorescence microscope (Olympus IX70). The number of cells was analyzed using ImageJ software.

For the invasion assay, after serum-starvation for 24 h, $4 \times 10^4$ cells were seeded as above in matrigel-sealed upper chambers (Corning) in serum-free medium. After incubation for 48 h at 37°C, non-invasive cells on the top surface of the filter were removed with cotton swabs. Invasive cells that migrated to the lower surface of the filter were fixed, stained and scored as described above.

For MCF10A cells, cells were transfected with apMNKQ2 and treated with 5 ng/mL TGF-β in medium with 0.5% horse serum for 48 h and $6 \times 10^4$ cells were seeded in upper chambers without or with matrigel (0.5 mg/mL) for migration or invasion assays respectively.

**Zymography**

Zymography was used to analyze MMP-2 and MMP-9 activity in the medium of MCF10A treated or untreated with TGF-β and apMNKQ2 after 48 h of incubation. Medium was collected and centrifuged at 210 g to remove cell debris. Twenty-five microliters of medium were mixed with loading buffer without mercaptoethanol and resolved on a 7.5% SDS-PAGE polyacrylamide gel co-polymerized with 1 mg/mL gelatin. Gels were incubated 30 min in 2.5% Triton X-100 at room temperature and overnight at 37°C in developing buffer (Tris 50 mM pH 7.5, NaCl 200 mM, $CaCl_2$ 5 mM, Tween 0.02%). Gels were stained with Coomassie blue for 15 min and destained until MMPs activity appeared as clear bands.

**Quantitative real-time PCR**

Total RNA prepared as described above was used for the obtention of first-strand cDNA using the SensiFAST cDNA Synthesis Kit (Bioline, Segovia, Spain). The reverse transcription reaction products were used for qPCR amplification, using AceQ qPCR SYBR Green Master Mix (Nanjing Vazyme Biotech, Nanjing, China) according to the manufacturer's instructions on a StepOne Plus Real-Time PCR system (Applied Biosystem, Waltham, MA). Triplicate reactions of the target gene and housekeeping gene were performed simultaneously for each cDNA template. The $2^{-\Delta\Delta Ct}$ method was used to calculate the relative expression of each target gene.[51] Thus, the data were normalized with respect to housekeeping mRNA (β-actin) levels and $\Delta Ct$ ($Ct_{target}-Ct_{housekeeping}$) values were determined. $\Delta\Delta Ct$ was calculated as $\Delta Ct_{apMNKQ2/experimental\ condition}-\Delta Ct_{control}$. Finally, data are expressed as $2^{-\Delta\Delta Ct}$. Oligonucleotides used in this work are listed in Table S2.

**Immunohistochemistry**

Tumor sections (5 μm) were deparaffinized and rehydrated as described previously[35] and antigen retrieval was achieved by heat treatment in a pressure cooker for 2 min in 10 mM citrate buffer (pH 6.5). Next, endogenous peroxidase was blocked, and the sections were incubated with anti-PCNA (Santa Cruz Biotechnology, Dallas, TX) 1:100 overnight at room temperature. Sections were incubated with Master Polymer Plus Detection System (Peroxidase) (Master Diagnostica, Granada, Spain) for 45 min and developed with the Immunoperoxidase DAB kit (Master Diagnostica) according to the manufacturer's instructions. Sections were counterstained with hematoxylin. Positive cells were analyzed using ImageJ software.

### Efficacy study in a triple-negative breast cancer orthotropic mouse model

Two independent studies were performed by Leitat (LEITAT Technological Center, Barcelona, Spain) and in our laboratory (Department of Biochemistry and Molecular Biology, Complutense University, Madrid, Spain) following a similar procedure. All animal procedures were performed with the approval of the Complutense University Animal Experimentation Committee and Madrid Regional Government, according to European official regulations. The strain of mice was Hsd:Athymic Nude-Foxn1nu. The animals were maintained in an air and temperature-controlled cages, with a regular supply of water and food. MDA-MB-231 cells were inoculated ($2.5$–$5 \times 10^6$ cells/animal respectively) in 50 µL DMEM or PBS into the fourth mammary fat pad mice. Once tumors were established (tumor volume of approximately 100 mm$^3$), tumor-bearing athymic mice were randomized (10 mice in each group) and treated as follows: (1) vehicle control (selection buffer: in vivo-jetPEI (Polypus, Illkirch, France), (2) 1.8–2 mg/kg apMNKQ2:in vivo-jetPEI (5% glucose containing 46 µg apMNKQ2 and 5.6 µL jetPEI transfectant [N/P ratio of 6]), and (3) 2 mg/kg everolimus (Sigma) three times per week by intravenous injection. Tumors were measured two or three times per week with calipers and the tumor volume was calculated by the formula: D $\times$ d2/2. The RTV was calculated using the following formula: RTV = (tumor volume on measured day)/(tumor volume on day 0). At the end of the treatment, the TGI ratio (%) was calculated using the following formula: TGI (%) = [1 − (RTV of the treated group)/(RTV of the control group)] $\times$ 100 (%). Animals were also weighed twice weekly and monitored for general health status and signs of possible toxicity because of the treatments. The mice were sacrificed after the indicated periods of treatment and the tumors were excised. Tumors were divided and frozen in liquid nitrogen for western blot and qPCR analysis or placed in 10% buffered formalin for immunohistochemistry.

For the efficacy assay in a breast cancer orthotopic mice model with spontaneous metastasis, performed by Leitat, the BALB/c mouse strain AnNHsd was used. 4T1 cells were inoculated ($2 \times 10^5$ cells/animal) in 50 µL DMEM into the fourth mammary fat pad of mice. Once tumors were established (average tumor size of 72.5 ± 4.7 mm$^3$), BALBc mice (10 mice in each group) were randomized and treated with 160 µL of vehicle control (selection buffer: in vivo-jetPEI) or 3.6 mg/Kg apMNKQ2:in vivo-jetPEI (73.6 µg apMNKQ2 and 7.4 µL jetPEI transfectant [N/P ratio of 5]) three times per week by intravenous injection. Tumor volume and animal weights were measured as above. At the end of treatment, tumors were excised and one-half frozen and one-half was fixed in formalin. In addition, the extraction of the lungs was performed for the assessment of the metastasis with the inverse tincture method with Chinese ink.

### Statistical analyses

Data are presented as mean value ± standard error of the mean. To determine whether differences between the averages of the different experimental groups were significant, statistical analysis was performed by ANOVA followed by Tukey's test, unpaired t test, or one-sample t test versus a control value with Graphpad Prism 8.0 (San Diego, CA). Significance was assumed at $p < 0.05$.

### Data availability statement

Data are contained within the article or Supplemental Information.

## AUTHOR CONTRIBUTIONS

Conceptualization, C.P-D, R.F-M, V.M.G., and M.E.M.; methodology, C.P.-.D, R.F.-M., R.C.-M., J.I.K.-M, M.G.-H, M.I.P.-M, S.S., M.B.-U., M.S.-V., I.T., S.B.-B., and I.G.-P.; investigation, C.P.-D., R.F.-M., E.P.-G., C.S.,C.G., V.M.G., and M.E.M.; writing—original draft preparation, C.P.-D., R.F.-M., V.M.G., and M.E.M.; writing—review and editing, C.P.-D., R.F.-M., V.M.G., and M.E.M. All authors have read and agreed to the published version of the manuscript.

## DECLARATION OF INTEREST

C.P.-D., R.F.-M., V.M.G., and M.E.M. declare that a patent application has been filed relating to this work.

## REFERENCES

1. Sung, H., Ferlay, J., Siegel, R.L., Laversanne, M., Soerjomataram, I., Jemal, A., and Bray, F. (2021). Global cancer statistics 2020: GLOBOCAN estimates of incidence and mortality worldwide for 36 cancers in 185 countries. CA. Cancer J. Clin. 71, 209–249. https://doi.org/10.3322/caac.21660.

2. Fukunaga, R., and Hunter, T. (1997). MNK1, a new MAP kinase-activated protein kinase, isolated by a novel expression screening method for identifying protein kinase substrates. EMBO J. 16, 1921–1933. https://doi.org/10.1093/emboj/16.8.1921.

3. O'Loghlen, A., González, V.M., Piñeiro, D., Pérez-Morgado, M.I., Salinas, M., and Martín, M.E. (2004). Identification and molecular characterization of Mnk1b, a splice

variant of human MAP kinase-interacting kinase Mnk1. Exp. Cell Res. *299*, 343–355. https://doi.org/10.1016/j.yexcr.2004.06.006.

4. O'Loghlen, A., González, V.M., Jurado, T., Salinas, M., and Martín, M.E. (2007). Characterization of the activity of human MAP kinase-interacting kinase Mnk1b. Biochim. Biophys. Acta *1773*, 1416–1427. https://doi.org/10.1016/j.bbamcr.2007.05.009.

5. Buxadé, M., Parra, J.L., Rousseau, S., Shpiro, N., Marquez, R., Morrice, N., Bain, J., Espel, E., and Proud, C.G. (2005). The Mnks are novel components in the control of TNF alpha biosynthesis and phosphorylate and regulate hnRNP A1. Immunity *23*, 177–189. https://doi.org/10.1016/j.immuni.2005.06.009.

6. Buxadé, M., Morrice, N., Krebs, D.L., and Proud, C.G. (2008). The PSF.p54nrb complex is a novel Mnk substrate that binds the mRNA for tumor necrosis factor alpha. J. Biol. Chem. *283*, 57–65. https://doi.org/10.1074/jbc.M705286200.

7. Hefner, Y., Borsch-Haubold, A.G., Murakami, M., Wilde, J.I., Pasquet, S., Schieltz, D., Ghomashchi, F., Yates, J.R., 3rd, Armstrong, C.G., Paterson, A., et al. (2000). Serine 727 phosphorylation and activation of cytosolic phospholipase A2 by MNK1-related protein kinases. J. Biol. Chem. *275*, 37542–37551. https://doi.org/10.1074/jbc.M003395200.

8. DaSilva, J., Xu, L., Kim, H.J., Miller, W.T., and Bar-Sagi, D. (2006). Regulation of sprouty stability by Mnk1-dependent phosphorylation. Mol. Cell Biol. *26*, 1898–1907. https://doi.org/10.1128/MCB.26.5.1898-1907.2006.

9. Pinto-Díez, C., Ferreras-Martín, R., Carrión-Marchante, R., González, V.M., and Martín, M.E. (2020). Deeping in the role of the MAP-kinases interacting kinases (MNKs) in cancer. Int. J. Mol. Sci. *21*, E2967. https://doi.org/10.3390/ijms21082967.

10. Wendel, H.G., Silva, R.L.A., Malina, A., Mills, J.R., Zhu, H., Ueda, T., Watanabe-Fukunaga, R., Fukunaga, R., Teruya-Feldstein, J., Pelletier, J., and Lowe, S.W. (2007). Dissecting eIF4E action in tumorigenesis. Genes Dev. *21*, 3232–3237. https://doi.org/10.1101/gad.1604407.

11. Topisirovic, I., Ruiz-Gutierrez, M., and Borden, K.L.B. (2004). Phosphorylation of the eukaryotic translation initiation factor eIF4E contributes to its transformation and mRNA transport activities. Cancer Res. *64*, 8639–8642. CAN-04-2677. https://doi.org/10.1158/0008-5472.

12. Culjkovic, B., Topisirovic, I., and Borden, K.L.B. (2007). Controlling gene expression through RNA regulons: the role of the eukaryotic translation initiation factor eIF4E. Cell Cycle *6*, 65–69. 3688 [pii].

13. Phillips, A., and Blaydes, J.P. (2008). MNK1 and EIF4E are downstream effectors of MEKs in the regulation of the nuclear export of HDM2 mRNA. Oncogene *27*, 1645–1649. https://doi.org/10.1038/sj.onc.1210785.

14. D'Abronzo, L.S., and Ghosh, P.M. (2018). eIF4E phosphorylation in prostate cancer. Neoplasia *20*, 563–573. https://doi.org/10.1016/j.neo.2018.04.003.

15. Fan, S., Ramalingam, S.S., Kauh, J., Xu, Z., Khuri, F.R., and Sun, S.Y. (2009). Phosphorylated eukaryotic translation initiation factor 4 (eIF4E) is elevated in human cancer tissues. Cancer Biol. Ther. *8*, 1463–1469.

16. Hou, S., Du, P., Wang, P., Wang, C., Liu, P., and Liu, H. (2017). Significance of MNK1 in prognostic prediction and chemotherapy development of epithelial ovarian cancer. Clin. Transl. Oncol. *19*, 1107–1116. https://doi.org/10.1007/s12094-017-1646-x.

17. Pinto-Díez, C., García-Recio, E.M., Pérez-Morgado, M.I., García-Hernández, M., Sanz-Criado, L., Sacristán, S., Toledo-Lobo, M.V., Pérez-Mies, B., Esteban-Rodríguez, I., Pascual, A., et al. (2018). Increased expression of MNK1b, the spliced isoform of MNK1, predicts poor prognosis and is associated with triple-negative breast cancer. Oncotarget *9*, 13501–13516. https://doi.org/10.18632/oncotarget.24417.

18. Santag, S., Siegel, F., Wengner, A.M., Lange, C., Bömer, U., Eis, K., Pühler, F., Lienau, P., Bergemann, L., Michels, M., et al. (2017). BAY 1143269, a novel MNK1 inhibitor, targets oncogenic protein expression and shows potent anti-tumor activity. Cancer Lett. *390*, 21–29. https://doi.org/10.1016/j.canlet.2016.12.029.

19. Bell, J.B., Eckerdt, F.D., Alley, K., Magnusson, L.P., Hussain, H., Bi, Y., Arslan, A.D., Clymer, J., Alvarez, A.A., Goldman, S., et al. (2016). MNK inhibition disrupts mesenchymal glioma stem cells and prolongs survival in a mouse model of glioblastoma. Mol. Cancer Res. *14*, 984–993. MCR-16-0172. https://doi.org/10.1158/1541-7786.

20. Wheater, M.J., Johnson, P.W., and Blaydes, J.P. (2010). The role of MNK proteins and eIF4E phosphorylation in breast cancer cell proliferation and survival. Cancer Biol. Ther. *10*, 728–735. https://doi.org/10.4161/cbt.10.7.12965.

21. Ueda, T., Watanabe-Fukunaga, R., Fukuyama, H., Nagata, S., and Fukunaga, R. (2004). Mnk2 and Mnk1 are essential for constitutive and inducible phosphorylation of eukaryotic initiation factor 4E but not for cell growth or development. Mol. Cell Biol. *24*, 6539–6549. https://doi.org/10.1128/MCB.24.15.6539-6549.2004.

22. Lineham, E., Spencer, J., and Morley, S.J. (2017). Dual abrogation of MNK and mTOR: a novel therapeutic approach for the treatment of aggressive cancers. Future Med. Chem. *9*, 1539–1555. https://doi.org/10.4155/fmc-2017-0062.

23. Jin, X., Yu, R., Wang, X., Proud, C.G., and Jiang, T. (2021). Progress in developing MNK inhibitors. Eur. J. Med. Chem. *219*, 113420. https://doi.org/10.1016/j.ejmech.2021.113420.

24. Abdelaziz, A.M., Yu, M., and Wang, S. (2021). Mnk inhibitors: a patent review. Pharm. Pat. Anal. *10*, 25–35. https://doi.org/10.4155/ppa-2020-0028.

25. Ellington, A.D., and Szostak, J.W. (1990). In vitro selection of RNA molecules that bind specific ligands. Nature *346*, 818–822. https://doi.org/10.1038/346818a0.

26. Tuerk, C., and Gold, L. (1990). Systematic evolution of ligands by exponential enrichment: RNA ligands to bacteriophage T4 DNA polymerase. Science *249*, 505–510.

27. Pereira, R.L., Nascimento, I.C., Santos, A.P., Ogusuku, I.E.Y., Lameu, C., Mayer, G., and Ulrich, H. (2018). Aptamers: novelty tools for cancer biology. Oncotarget *9*, 26934–26953. https://doi.org/10.18632/oncotarget.25260.

28. Ruiz Ciancio, D., Vargas, M.R., Thiel, W.H., Bruno, M.A., Giangrande, P.H., and Mestre, M.B. (2018). Aptamers as diagnostic tools in cancer. Pharmaceuticals *11*, E86. https://doi.org/10.3390/ph11030086.

29. Zhou, J., and Rossi, J. (2017). Aptamers as targeted therapeutics: current potential and challenges. Nat. Rev. Drug Discov. *16*, 181–202. https://doi.org/10.1038/nrd.2016.199.

30. Xiao, X., Li, H., Zhao, L., Zhang, Y., and Liu, Z. (2021). Oligonucleotide aptamers: recent advances in their screening, molecular conformation and therapeutic applications. Biomed. Pharmacother. *143*, 112232. https://doi.org/10.1016/j.biopha.2021.112232.

31. García-Recio, E.M., Pinto-Díez, C., Pérez-Morgado, M.I., García-Hernández, M., Fernández, G., Martín, M.E., and González, V.M. (2016). Characterization of MNK1b DNA aptamers that inhibit proliferation in MDA-MB231 breast cancer cells. Mol. Ther. Nucleic Acids *5*, e275. https://doi.org/10.1038/mtna.2015.50.

32. Evans, M.K., Brown, M.C., Geradts, J., Bao, X., Robinson, T.J., Jolly, M.K., Vermeulen, P.B., Palmer, G.M., Gromeier, M., Levine, H., et al. (2018). XIAP regulation by MNK links MAPK and NFkappaB signaling to determine an aggressive breast cancer phenotype. Cancer Res. *78*, 1726–1738. https://doi.org/10.1158/0008-5472.CAN-17-1667.

33. Zhao, M., Mishra, L., and Deng, C.X. (2018). The role of TGF-beta/SMAD4 signaling in cancer. Int. J. Biol. Sci. *14*, 111–123. https://doi.org/10.7150/ijbs.23230.

34. Chiang, S.P.H., Cabrera, R.M., and Segall, J.E. (2016). Tumor cell intravasation. Am. J. Physiol. Cell Physiol. *311*, C1–C14. https://doi.org/10.1152/ajpcell.00238.2015.

35. Viglasky, V., and Hianik, T. (2013). Potential uses of G-quadruplex-forming aptamers. Gen. Physiol. Biophys. *32*, 149–172. https://doi.org/10.4149/gpb_2013019.

36. Xie, J., Merrett, J.E., Jensen, K.B., and Proud, C.G. (2019). The MAP kinase-interacting kinases (MNKs) as targets in oncology. Expert Opin. Ther. Targets *23*, 187–199. https://doi.org/10.1080/14728222.2019.1571043.

37. Kumar, K., Chow, C.R., Ebine, K., Arslan, A.D., Kwok, B., Bentrem, D.J., Eckerdt, F.D., Platanias, L.C., and Munshi, H.G. (2016). Differential regulation of ZEB1 and EMT by MAPK-interacting protein kinases (MNK) and eIF4E in pancreatic cancer. Mol. Cancer Res. *14*, 216–227. https://doi.org/10.1158/1541-7786.MCR-15-0285.

38. Stemmler, M.P., Eccles, R.L., Brabletz, S., and Brabletz, T. (2019). Non-redundant functions of EMT transcription factors. Nat. Cell Biol. *21*, 102–112. https://doi.org/10.1038/s41556-018-0196-y.

39. Liu, T.A., Jan, Y.J., Ko, B.S., Liang, S.M., Chen, S.C., Wang, J., Hsu, C., Wu, Y.M., and Liou, J.Y. (2013). 14-3-3epsilon overexpression contributes to epithelial-mesenchymal transition of hepatocellular carcinoma. PLoS One *8*, e57968. https://doi.org/10.1371/journal.pone.0057968.

40. Nakamura, R., Ishii, H., Endo, K., Hotta, A., Fujii, E., Miyazawa, K., and Saitoh, M. (2018). Reciprocal expression of Slug and Snail in human oral cancer cells. PLoS One *13*, e0199442. https://doi.org/10.1371/journal.pone.0199442.

41. Puisieux, A., Brabletz, T., and Caramel, J. (2014). Oncogenic roles of EMT-inducing transcription factors. Nat. Cell Biol. *16*, 488–494. https://doi.org/10.1038/ncb2976.

42. Maeda, M., Johnson, K.R., and Wheelock, M.J. (2005). Cadherin switching: essential for behavioral but not morphological changes during an epithelium-to-mesenchyme transition. J. Cell Sci. *118*, 873–887. https://doi.org/10.1242/jcs.01634.

43. Chen, A., Beetham, H., Black, M.A., Priya, R., Telford, B.J., Guest, J., Wiggins, G.A.R., Godwin, T.D., Yap, A.S., and Guilford, P.J. (2014). E-cadherin loss alters cytoskeletal organization and adhesion in non-malignant breast cells but is insufficient to induce an epithelial-mesenchymal transition. BMC Cancer *14*, 552. https://doi.org/10.1186/1471-2407-14-552.

44. Konicek, B.W., Stephens, J.R., McNulty, A.M., Robichaud, N., Peery, R.B., Dumstorf, C.A., Dowless, M.S., Iversen, P.W., Parsons, S., Ellis, K.E., et al. (2011). Therapeutic inhibition of MAP kinase interacting kinase blocks eukaryotic initiation factor 4E phosphorylation and suppresses outgrowth of experimental lung metastases. Cancer Res. *71*, 1849–1857. https://doi.org/10.1158/0008-5472.

45. Sussman, A., Huss, K., Chio, L.C., Heidler, S., Shaw, M., Ma, D., Zhu, G., Campbell, R.M., Park, T.S., Kulanthaivel, P., et al. (2004). Discovery of cercosporamide, a known antifungal natural product, as a selective Pkc1 kinase inhibitor through high-throughput screening. Eukaryot. Cell *3*, 932–943. https://doi.org/10.1128/EC.3.4.932-943.2004.

46. Hou, J., Lam, F., Proud, C., and Wang, S. (2012). Targeting Mnks for cancer therapy. Oncotarget *3*, 118–131. https://doi.org/10.18632/oncotarget.453.

47. Xu, W., Kannan, S., Verma, C.S., and Nacro, K. (2022). Update on the development of MNK inhibitors as therapeutic agents. J. Med. Chem. *65*, 983–1007. https://doi.org/10.1021/acs.jmedchem.1c00368.

48. Ramalingam, S., Gediya, L., Kwegyir-Afful, A.K., Ramamurthy, V.P., Purushottamachar, P., Mbatia, H., and Njar, V.C.O. (2014). First MNKs degrading agents block phosphorylation of eIF4E, induce apoptosis, inhibit cell growth, migration and invasion in triple negative and Her2-overexpressing breast cancer cell lines. Oncotarget *5*, 530–543. https://doi.org/10.18632/oncotarget.1528.

49. Mbatia, H.W., Ramalingam, S., Ramamurthy, V.P., Martin, M.S., Kwegyir-Afful, A.K., and Njar, V.C.O. (2015). Novel C-4 heteroaryl 13-cis-retinamide Mnk/AR degrading agents inhibit cell proliferation and migration and induce apoptosis in human breast and prostate cancer cells and suppress growth of MDA-MB-231 human breast and CWR22Rv1 human prostate tumor xenografts in mice. J. Med. Chem. *58*, 1900–1914. https://doi.org/10.1021/jm501792c.

50. Ramalingam, S., Ramamurthy, V.P., Gediya, L.K., Murigi, F.N., Purushottamachar, P., Huang, W., Choi, E.Y., Zhang, Y., Vasaitis, T.S., Kane, M.A., et al. (2019). The novel Mnk1/2 degrader and apoptosis inducer VNLG-152 potently inhibits TNBC tumor growth and metastasis. Cancers *11*, E299. https://doi.org/10.3390/cancers11030299.

51. Livak, K.J., and Schmittgen, T.D. (2001). Analysis of relative gene expression data using real-time quantitative PCR and the 2(-Delta Delta C(T)) Method. Methods *25*, 402–408. https://doi.org/10.1006/meth.2001.1262.